A micromechanical muUNSAT effective stress expression for stress-strain behaviour of wet granular materials

Jérôme Duriez, R. Wan

Author-produced version of the article published in Geomechanics for Energy and the Environment, 2018, 15, 10-18
The original publication is available at https://www.sciencedirect.com/science/article/pii/S2352380817300357
DOI: 10.1016/j.gete.2017.12.003

A micromechanical μUNSAT effective stress expression for stress-strain behaviour of wet granular materials

J. Duriez[a,b,*], R. Wan[a]

[a] *University of Calgary, Calgary, AB, T2N 1N4, Canada*
[b] *Irstea, UR RECOVER, F-13182 Aix-en-Provence, France*

Abstract

The definition of an effective stress variable for idealized triphasic granular media as the contact stress arising from interparticle forces is examined through discrete element modelling computations in concert with appropriately derived analytical stress expressions based on homogenization. The latter take a more practical importance, in that they also circumvent the need for direct measurements of interparticle contact forces. Considering dry or pendular-regime conditions for slightly polydisperse dense and loose packings, the contact stress-strain behaviours in dry or wet conditions are compared along a variety of loading paths, depending on the level of plastic dissipation involved. The contact stress indeed emerges as an effective stress variable with a remarkable stress-strain character along contractant loading paths and for dense solid packings where the behaviour is close to be non-dissipative. Along more dilatant loading paths or for looser packings, plastic dissipation increases and the coincidence of the constitutive behaviour in both dry and triphasic conditions is restricted to the initial stages of the loading paths, limiting the applicability of the contact stress to the estimation of initial stiffnesses. The stark constitutive differences between the proposed effective stress and Bishop's stress are also highlighted.

Keywords: effective stress, Discrete Element Method (DEM), granular, pendular, μUNSAT

*Corresponding author
Email address: jerome.duriez@irstea.fr (J. Duriez)

1. Introduction

Energy and Environmental Engineering operations require a precise mechanical description of multiphase porous media such as in oil and gas reservoirs, or partially water-saturated (unsaturated) soils. Obviously, the presence of various fluids within the pore space network of these multiphasic materials greatly modifies their mechanical behaviour with respect to the dry (air-saturated) state which is well understood. For biphasic (or two-phase) porous media penetrated by a single pore fluid, a unified mechanical description by way of dry state constitutive models actually exists whatever the pore fluid and its pressure are following Terzaghi's and Biot's effective stress equations [1, 2]. Turning to triphasic (or three-phase) conditions with an immiscible fluid mixture, it would also be highly beneficial to extend this effective stress concept so that triphasic materials can be described by just inserting an adequate single effective stress into models designed for dry materials. In other words, the objective is to obtain a stress-strain-strength effective stress that would allow failure criterion and constitutive relations from dry conditions, all together, to be applied to triphasic conditions in order to easily predict limit stress states and strains. However, the exact determination of such a single effective stress has revealed to be highly challenging ever since the early Bishop's attempts [3].

When describing failure in triphasic media, it has been often possible to resort to an effective stress framework based on limit stress states according to dry shear strength criteria [4, 5, 6, 7, 8]. In these works, the effective stress is either phenomenologically deduced from Bishop's equation with appropriate expressions for χ coefficient [4, 7], or as the contact forces stress contribution which can be indirectly accessed by subtracting a so-called suction stress from the total stress [5, 6, 8]. The suction stress [5] encompasses all relevant stress contributions in triphasic materials, excluding the contact stress stemming from the contact forces between the solid grains of the skeleton, and can be identified for granular materials with the capillary stress since other physico-chemical forces are then negligible. As for the contact stress, the latter appears as a logical stress-strength effective stress since pore water is reported to have little or no influence onto the contact-scale local frictional threshold [9, 10], which thus leads to unique limit states for the macroscopic contact stress and a unified failure description irrespective of saturation.

Whereas in the biphasic case unique constitutive relations are related to strains via Biot's effective stress, no effective stress has yet been found that would relate to strains in triphasic conditions through dry constitutive relations [7]. As such, the application of an effective stress principle to triphasic materials has often been challenged since Bishop himself [3], with alternate approaches relying on total stress and another stress variable such as matric suction to describe unsaturated conditions using additional constitutive equations that are specific to these triphasic conditions [11, 12]. A compromise may, nevertheless, be found in that quasi-elastic behaviour, e.g. volume change along overconsolidated œdometric loadings, may still be described in triphasic conditions using an effective stress framework [4, 13, 14]. Recent micromechanical results by the authors [8, 15] suggest that the same contact stress also enjoys such a quasi-elastic strain-stress effective nature, in addition to its stress-strength character. This seems to be indeed coherent because granular material strains derive from solid particle relative displacements that relate to contact forces through a unique contact law, irrespective of saturation.

The present work aims to provide new evidences that demonstrate the stress-strain effective character of the contact stress in any regime showing small plastic dissipation by considering a wide range of loading paths which were absent from previous studies [8, 15].

It is further noted that direct measurements of contact forces and contact stresses are still beyond reach in triphasic materials in spite of a current research in the field [16]. To address this shortcoming, the present paper first recalls in Section 2 the μUNSAT expressions that enable one to indirectly access the contact stress through capillary stresses and the fluid phase microstuctures, whose measurements appear to be more feasible thanks to e.g. computed tomography [17, 18]. For the purpose of the paper, the choice is actually made to consider a Discrete Element Method (DEM) model for wet granular materials [19], presented in Section 3, which allows both direct and indirect measurements of the contact stress from a comprehensive description of the microstructure of all solid and fluid phases, including interfaces. Numerical comparisons of dry-wet behaviours for slightly polydisperse materials along various loading paths are then presented in Section 4, validating the stress-strain effective nature of the contact stress in regimes with small dissipation, and hence the present μUNSAT effective stress expression. Section 5 finally evidences the fundamental differences in the pendular regime between the present μUNSAT effective stress and Bishop's stress, whose inapplicability to wet conditions is once again demonstrated.

2. Micromechanical μUNSAT effective stress expression

2.1. Total stress decomposition from micromechanics

The μUNSAT approach expresses the contact stress by isolating from the macroscopic total stresses $\boldsymbol{\Sigma}$, all microscopic stress contributions due to the various phases and interfaces that encompass triphasic granular media. First, the solid s and fluid (n, w) bulk phases are considered with their corresponding volumes V_s, V_n and V_w. Here, n stands for the non-wetting fluid, e.g. air, whereas w refers to the wetting one, e.g. water. Additionally, all three interfaces $S_{\alpha\beta}$, $\alpha, \beta = n, s, w$ are as well included in the approach since the corresponding surface tensions $\gamma_{\alpha\beta}$ necessarily belong to the internal forces of the triphasic material. As such, the total stresses are given as follows:

$$\boldsymbol{\Sigma} = \frac{1}{V}\left(\sum_{\alpha=n,s,w}\int_{V_\alpha}\boldsymbol{\sigma_\alpha}\,dV + \sum_{\alpha,\beta=n,s,w}\int_{S_{\alpha\beta}}\boldsymbol{\pi_{\alpha\beta}}\,dS\right) \tag{1}$$

In Eq. (1), the fluid stresses $\boldsymbol{\sigma_\alpha}$, $\alpha = n, w$, are directly given by the corresponding pressures $u_\alpha\,\boldsymbol{\delta}$ with $\boldsymbol{\delta}$ as the identity tensor, whereas the solid stress $\boldsymbol{\sigma_s}$ can be classically expressed in terms of the tractions acting along the solid particles surfaces S_p [20]. The surface stress tensors $\boldsymbol{\pi_{\alpha\beta}} = \gamma_{\alpha\beta}\,(\vec{n}\otimes\vec{n} - \boldsymbol{\delta})$, with $\vec{n}$ as the normal to $S_{\alpha\beta}$, finally describe the surface tension fields acting as internal forces within any interface $S_{\alpha\beta}$ [21, 22, 23, 24].

Algebraic manipulations applied to Eq. (1) lead to the following μUNSAT decomposition of $\boldsymbol{\Sigma}$ into the contact stress $\boldsymbol{\sigma^{cont}}$ and the capillary stress $\boldsymbol{\sigma^{cap}}$, to which the solid fluid surface tensions $\gamma_{s\alpha}$ eventually do not contribute in the case of rigid solid particles [20, 22, 24]:

$$\boldsymbol{\Sigma} - u_n\, \boldsymbol{\delta} = \boldsymbol{\sigma^{cont}} + \boldsymbol{\sigma^{cap}} \tag{2}$$

$$\boldsymbol{\sigma^{cont}} = \frac{1}{V} \sum_c \vec{f^c} \otimes \vec{l} \tag{3}$$

$$\begin{aligned}
\boldsymbol{\sigma^{cap}} &= -\frac{1}{V}\Bigg[u_c \left(V_w\, \boldsymbol{\delta} + \int_{S_{sw}} \vec{n} \otimes \vec{x}\; dS \right) \\
&\qquad + \gamma_{nw} \left(\int_{S_{nw}} (\boldsymbol{\delta} - \vec{n} \otimes \vec{n})\; dS + \int_{\Gamma} \vec{\nu} \otimes \vec{x}\; dl \right) \Bigg] \\
&= -\frac{1}{V}\Big[u_c \left(\boldsymbol{\mu_{Vw}} + \boldsymbol{\mu_{Ssw}} \right) + \gamma_{nw} \left(\boldsymbol{\mu_{Snw}} + \boldsymbol{\mu_{\Gamma}} \right) \Big]
\end{aligned} \tag{4}$$

Eq. (3) refers to the standard definition of the contact stress tensor $\boldsymbol{\sigma^{cont}}$ from the contact forces $\vec{f^c}$ between solid particles, and the corresponding branch vector $\vec{l}$ connecting the centroids of contacting particles.

In Eq. (4), the capillary stress $\boldsymbol{\sigma^{cap}}$ encompasses the remainder of the internal forces that arise both from the fluid-fluid surface tension γ_{nw} and the capillary pressure $u_c = u_n - u_w$ that is equal to suction in granular materials. Four microstructure tensors $\boldsymbol{\mu_X}$ reflect the tensorial nature of these internal forces, with $\boldsymbol{\mu_{Vw}}$ the only one being always spherical since it corresponds to the isotropic action of suction within V_w. Other microstructure tensors have a general, non-spherical, tensorial expression with e.g. $\boldsymbol{\mu_{Ssw}}$ depending on the orientation of the wetted surface S_{sw} since the latter sustains suction along its normal only. Also, $\boldsymbol{\mu_{Snw}}, \boldsymbol{\mu_{\Gamma}}$ reflect the orientations of the interface S_{nw} and of the three-phase contact lines Γ that are subjected to fluid-fluid surface tension, where $\vec{\nu}$ in Eq. (4) is the tangent to S_{nw} being normal to Γ [20].

2.2. μUNSAT contact stress expression

Isolating $\boldsymbol{\sigma^{cont}}$ in Eq. (2)-(4), the following μUNSAT expression for the contact stress is eventually obtained:

$$\boldsymbol{\sigma^{cont}} = \boldsymbol{\Sigma} - u_n\, \boldsymbol{\delta} + \frac{1}{V}\Big[u_c \left(\boldsymbol{\mu_{Vw}} + \boldsymbol{\mu_{Ssw}} \right) + \gamma_{nw} \left(\boldsymbol{\mu_{Snw}} + \boldsymbol{\mu_{\Gamma}} \right) \Big] \tag{5}$$

Such an expression is believed to provide an easier access to $\boldsymbol{\sigma}^{\boldsymbol{cont}}$ during experiments than the direct definition of Eq. (3). Imaging techniques such as computed tomography indeed are very promising in allowing precise measurements of the fluid phase microstructures [17, 18]. Then, one would be able to compute the microstructure tensors $\boldsymbol{\mu}_{\boldsymbol{X}}$ in Eq. (5), as opposed to requiring more complex contact force measurements [16] that enter the direct contact stress expression, Eq. (3).

Leaving any experimental endeavour aside for now, Eq. (5) is herein used within the framework of DEM to investigate the very role of the contact stress in connection with strains, and whether it may serve as a strain-stress-strength effective stress expression.

3. DEM multiscale modelling of triphasic granular materials

Numerical DEM models indeed provide a convenient multiscale description of triphasic granular materials whereby the microstructure of all solid and fluid phases is easily measured. As such, the contact stress can be readily estimated using either Eq. (3) or (5) along various loading paths and for different packings.

3.1. Model formulation

Previously proposed in [19] and implemented in the Yade code [25], the considered DEM model addresses the case of spherical solid particles and a wetting fluid distribution in terms of distinct capillary bridges, i.e. menisci between particles pairs (Fig. 1), in accordance with the so-called pendular regime, also referred to as wet conditions. Such conditions correspond to a low wetting saturation, S_w, only, where S_w is defined as:

$$S_w = \frac{V_w}{V_w + V_n} \tag{6}$$

In line with another DEM approach [26], the model does not compute any biphasic pore flow, but instead assumes thermodynamic equilibrium and uniform capillary pressure conditions. As such, the menisci properties are computed

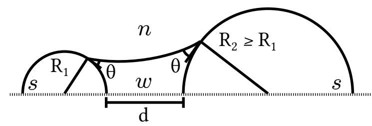

Figure 1: A capillary bridge

from the following Laplace-Young equation (7) which relates capillary pressure to surface tension and the interface curvature div $(\vec{n})$, with $\vec{n}$ being the normal to S_{nw} pointing from n to w:

$$u_c = \gamma_{nw} \ \mathrm{div}\,(\vec{n}) \tag{7}$$

According to the thermodynamic equilibrium assumption, Eq. (7) is solved for uniform values of u_c throughout the sample, also considering a uniform and constant contact angle θ (Fig. 1) [19]. As discussed in greater depth in [19], Eq. (7) is actually solved depending on the particles radii and their distance, in addition to imposed u_c and θ. Based on the S_{nw} interface profile, the numerical solution procedure finally outputs the resultant capillary force $\vec{f}^{cap}$ and other relevant microstructural quantities such as $\boldsymbol{\mu_{S_{nw}}} = \int_{S_{nw}} (\boldsymbol{\delta} - \vec{n} \otimes \vec{n}) \, dS$ for instance, thus enabling one to apply the μUNSAT Eq. (5) and measure contact stresses during DEM simulations [19].

The model actually inserts capillary bridges at each new contact between solid particles, with properties given by the Laplace-Young equation. In the instance the particles subsequently separate, the capillary bridge remains until some limit distance beyond which the Laplace-Young equation does not yield any solution. This hysteretic mechanism of bridge formation and rupture is consistent with experimental observations [27] and occurs in the model in a fully drained manner. The presence of a capillary bridge between two particles corresponds to a capillary interaction with the corresponding attractive capillary force $\vec{f}^{cap}$ due to the capillary pressure and surface tension loadings along the wetted surfaces S_{sw} and the contact lines Γ.

In addition, the interaction between touching particles is governed by classical elastic-plastic frictional (cohesionless) contact laws whereby normal and tangential relative displacements between particles are restricted by normal and tangential contact forces f_n^c and f_t^c [8, 19]. A simplified linear elastic behaviour of the contact interaction is first defined by the normal and tangential local stiffnesses, k_n and k_t, which are directly obtained from the average diameter $\bar{D}$ of any pair of contacting particles and the model parameters $k_n/\bar{D}$ and k_t/k_n:

$$k_n = \frac{k_n}{\bar{D}}\bar{D} \tag{8}$$

$$k_t = \frac{k_t}{k_n}k_n \tag{9}$$

with the consideration of an elastic shear stiffness being eventually restricted by the following Coulombian friction threshold, with μ the friction coefficient:

$$|f_t^c| \leqslant \mu\, f_n^c \tag{10}$$

Table 1 lists all parameters of the DEM model. The retained values for the contact interaction parameters, $k_n/\bar{D}$ and k_t/k_n, are similar to previous studies [8, 24, 19, 20]. As for the capillary interaction, the latter is fully determined by the fluid-fluid surface tension γ_{nw}, the contact angle θ and the particle size distribution. Air-water surface tension at ambient temperature is considered for γ_{nw} while a low though not zero θ-value corresponds to the wetting of glass beads by water, having at the same time the convenience of enhancing the mechanical effects of triphasic conditions [19]. Finally, silt-like particle diameters are chosen with a narrow particle size distribution being uniform in number between D_{min} and D_{max}.

Contact			Capillarity		Packing	
$k_n/\bar{D}$	k_t/k_n	μ	γ_{nw}	θ	D_{min}	D_{max}
(MPa)	(-)	(-)	(N/m)	(°)	(μm)	(μm)
10	0.5	0.5	0.073	10	21	25

Table 1: DEM model parameters

While the dynamic scheme of the DEM is classically carried out using some numerical damping, in order to obtain more easily a quasi-static evolution of the system, the damping coefficient [25] is taken as low as 0.05 to avoid numerical artifacts. Quasi-staticity is systematically verified through low values of the particle unbalanced forces [25] which were below 1% during all loading cases. As such, particle inertia (mass) does not play any role in the computations, which allows the use of density scaling with an artificially high density value (ρ = 20,000 kg/m^3 instead of 2,600 kg/m^3) for the particles. Without any consequence on the quasi-static rheology, density scaling reduces computational costs through larger time steps, even though loading rates have to be marginally reduced for quasi-staticity to still hold.

The DEM sample is a parallelepiped, initially a cube approximately 0.6 mm a side depending on packing density, with 6 rigid walls that enclose a total number of 20,000 spherical Discrete Elements (DE). Similar numbers (10,000 to 20,000) are classically used in material-scale DEM analyses [26, 19, 20, 28] in order to avoid numerical result dispersion from one numerical sample to another as well as field heterogeneity, in conformity with the Representative Elementary Volume (REV) concept. The DE sample is packed at various levels to produce different states in density as quantified by the porosity n and the average coordination number z_c:

$$n = \frac{V_n + V_w}{V_s + V_n + V_w} = \frac{V_v}{V} \tag{11}$$

$$z_c = \frac{2\,N_c - N_1}{N_p - N_1 - N_0} \tag{12}$$

with N_c the total number of contacts, and $N_0 + N_1$ the number of excluded rattlers, i.e. particles with zero or only one contact, and N_p the total number of DE. All considered packings are initially isotropic and prepared such that dry vs wet comparisons can be conducted in an unbiaised manner.

Care is indeed taken in considering dry or wet solid packings to be comparable in terms of n and z_c as these parameters obviously affect the dry constitutive relation which should also be described in wet conditions by an effective stress. As such, an appropriate particle packing generation procedure is followed which first involves a classical isotropic compression until a desired confining pressure is reached to obtain dense or loose dry packings [26], without the consideration of any capillary interaction that is only introduced in a second stage for the wet samples. In this manner, wet packings show initial states which are barely affected by the presence of capillary forces, and thus compare well with dry packings.

3.2. Dry and wet strain proportional loading paths

In order to investigate the stress-strain effective nature of the contact stress, the DEM model is used to explore the existence of a unique constitutive relation $\mathcal{F}$ between $\boldsymbol{\sigma^{cont}}$ and the strains $\boldsymbol{\varepsilon}$ in both dry (biphasic) and wet (triphasic) conditions. In the case of such an existence, $\mathcal{F}$ by definition would relate the current contact stress $\boldsymbol{\sigma^{cont}}(t)$ to the strain loading path $[\boldsymbol{\varepsilon}(\tau); -\infty < \tau \leqslant t]$ such that:

$$\boldsymbol{\sigma^{cont}}(t) = \mathcal{F}\big([\boldsymbol{\varepsilon}(\tau); -\infty < \tau \leqslant t]\big) \tag{13}$$

Extending our previous work [8, 15] where classical triaxial paths were examined, the validity of the same Eq. (13) in dry and wet conditions with a unique $\mathcal{F}$ is herein probed considering axisymmetric strain proportional loading paths, with '1' as the axis of symmetry and '2, 3' the two other spatial directions:

$$d\varepsilon_1 = cst \geqslant 0 \; ; \; d\varepsilon_2 = d\varepsilon_3 \; ; \; d\varepsilon_1 + 2\,R\,d\varepsilon_3 = 0 \tag{14}$$

The loading parameter $R \geqslant 0$ is constant along a given path, $R = 1$ corresponds to an isochoric loading path, whereas dilatancy (resp. contractancy) is imposed for $0 < R < 1$ (resp. $R > 1$). The limiting case $R = 0$ is defined as another contractant path ($d\varepsilon_1 = 0 \; ; \; d\varepsilon_2 = d\varepsilon_3 = cst \geqslant 0$).

Let's denote the volumetric strain as ε_V:

$$\varepsilon_V = \varepsilon_1 + 2\,\varepsilon_3 \tag{15}$$

and choose $||\boldsymbol{\varepsilon}||$ (the Euclidean norm of $\boldsymbol{\varepsilon}$) as a monotonously increasing loading parameter, i.e.

$$||\boldsymbol{\varepsilon}|| = \sqrt{{\varepsilon_1}^2 + 2\,{\varepsilon_3}^2} \tag{16}$$

Accordingly, Fig. 2 illustrates the corresponding dilatancy rates of four loading paths with $R \in \{0; 0.2; 1; 5\}$ that will be considered in the following analysis. In all cases, imposed strain rates are low enough to ensure quasi-static simulations

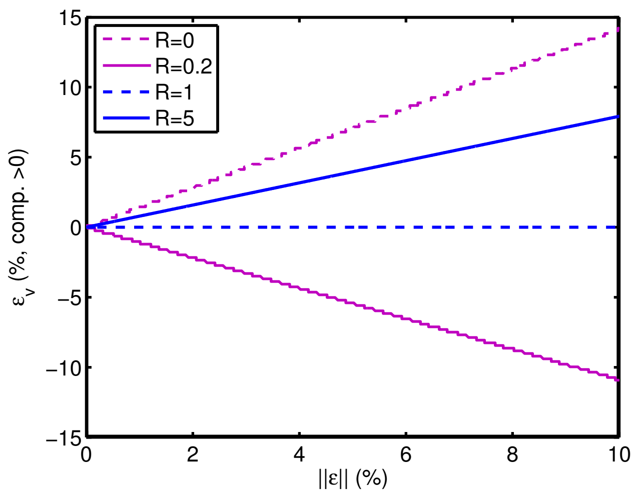

Figure 2: Dilatancy rates of imposed loading paths for $R \in \{0; 0.2; 1; 5\}$

as verified from the corresponding low values of the particle unbalanced forces [25] which were below 1%.

The main objective of imposing such strain loading paths on both dry and wet packings is to verify the hypothesis, $\boldsymbol{\sigma'} = \boldsymbol{\sigma^{cont}}$, upon which is founded the μUNSAT framework. If Eq. (13) holds, then the resulting contact stress paths should coincide in both dry and wet conditions. Recognizing the axial symmetry of the problem, it is convenient to associate the tensor $\boldsymbol{\sigma^{cont}}$ with the two classical scalars (invariants) p^{cont} and q^{cont}, i.e.

$$p^{cont} = \frac{\sigma_1^{cont} + 2\,\sigma_3^{cont}}{3} \tag{17}$$

$$q^{cont} = \sigma_1^{cont} - \sigma_3^{cont} \tag{18}$$

while similarly, p and q variables pertain to the total stress tensor $\boldsymbol{\Sigma}$:

$$p = \frac{\Sigma_1 + 2\,\Sigma_3}{3} \tag{19}$$

$$q = \Sigma_1 - \Sigma_3 \tag{20}$$

4. Validity of the μUNSAT effective stress

4.1. Dense packings

Proportional strain loading paths are first imposed to dense solid packings. In essence, the same strain loading path is imposed to similarly dense packings in both dry and wet conditions with the resulting contact stress paths recorded. The contact stress obviously coincides with the total stress in dry conditions, whereas Eq. (3) or (5) can be indistinctly used to access the contact stress under wet conditions [28].

Four strain loading paths are considered with $R \in \{0; 0.2; 1; 5\}$, under two different confining pressures referred to as "A" and "B". For each confining pressure A or B, and each R value, one dry and one wet test are considered, leading to 16 tests on dense packings in total. Table 2 gives details of the initial conditions for the dry-wet test pairs A, B pertaining to dense packings. These initial conditions are such that dry and wet tests of a given pair A or B show initial states $(\boldsymbol{\sigma^{cont}}, n, z_c)$ being as close as possible.

	Tests A		Tests B	
	Dry	Wet	Dry	Wet
Initial p (kPa)	11.1	2	20.6	10
Imposed u_c (kPa)	—	25	—	125
Initial S_w (%)	—	7.18	—	0.85
Initial n (-)	0.375	0.380	0.370	0.373
Initial z_c (-)	6.41	6.21	6.62	6.52

Table 2: Tests data for the dry and wet loading paths imposed on dense packings

Comparing the contact stress responses in dry and wet conditions (Fig. 3 and 4), it is indeed verified that virtually unique behaviours are observed along the contractant or isochoric loading paths $R \in \{0; 1; 5\}$. As such, this establishes the validity of using the dry constitutive relation $\mathcal{F}$ together with $\boldsymbol{\sigma^{cont}}$ as an effective stress along these loading paths.

As for the dilatant loading path $R = 0.2$, a unique behaviour is observed in the early stage of the test. Subsequently, the imposed dilatancy rate requires the stresses to eventually vanish in the dry case, whereas when wet the same packing

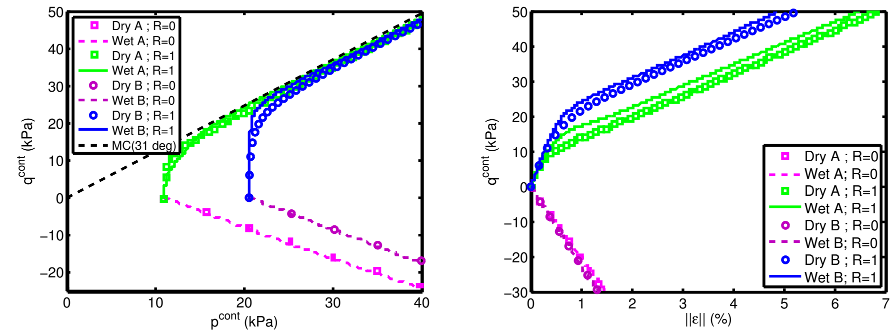

Figure 3: Contact stress response of a dense packing (Table 2) along contractant ($R = 0$) and isochoric ($R = 1$) strain loading paths (color version online)

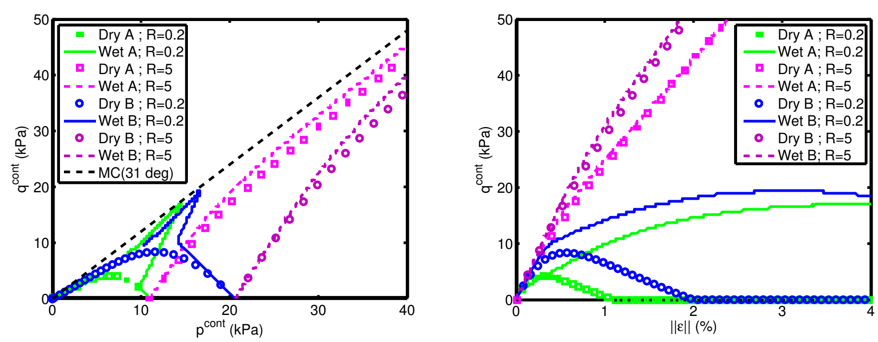

Figure 4: Contact stress response of a dense packing (Table 2) along contractant ($R = 5$) and dilatant ($R = 0.2$) strain loading paths (color version online)

gains a propensity to dilate originating from liquid bridges, thus avoiding a loss in bearing capacity. Hence, for such a dilatant loading path, the role of the contact stress as an effective stress is limited to the initial part of the loading path, and could still be used to predict initial stiffnesses in triphasic conditions.

It is noted that all contact stress responses obtained in both dry and triphasic conditions are found to be bounded by the same cohesionless Mohr-Coulomb failure criterion (with $c = 0$ Pa ; $\varphi = 31°$) that was previously measured in dry conditions for such packings [15]. The universal property of this limit stress line, irrespective of the phase condition, is another illustration of the previously mentioned stress-strength effective nature of the contact stress.

4.2. Loose packing

The same analysis procedure is now applied to loose packings (Table 3). The numerical results displayed in Figs. 5 and 6 reveal less of an agreement between dry and wet behaviours in comparison to the previous dense case study.

	Tests A		Tests B	
	Dry	Wet	Dry	Wet
Initial p (kPa)	8.1	2	17.3	10
Imposed u_c (kPa)	—	25	—	125
Initial S_w (%)	—	4.17	—	0.50
Initial n (-)	0.442	0.441	0.436	0.438
Initial z_c (-)	4.96	4.84	5.17	5.12

Table 3: Tests data for the dry and wet loading paths imposed on loose packings

In particular, the existence of a unique constitutive relation $\mathcal{F}$ between $\boldsymbol{\sigma^{cont}}$ and $\boldsymbol{\varepsilon}$ is identified for the most contractant loading path $R = 0$ only, and is somewhat approximated along the less contractant path $R = 5$.

As for the isochoric path $R = 1$, and at variance with the dense packing (Fig. 3), a dry-wet agreement is only obtained for the very initial phase during which p^{cont} remains constant, consistent with a possible relationship between $\boldsymbol{\sigma^{cont}}$ and $\boldsymbol{\varepsilon}$ through Hooke's elastic law. Then, the dry packing presents a 'liquefaction' behaviour with vanishing stresses, consistent with the constant volume condition and the underlying material contractant flow rule. In contrast,

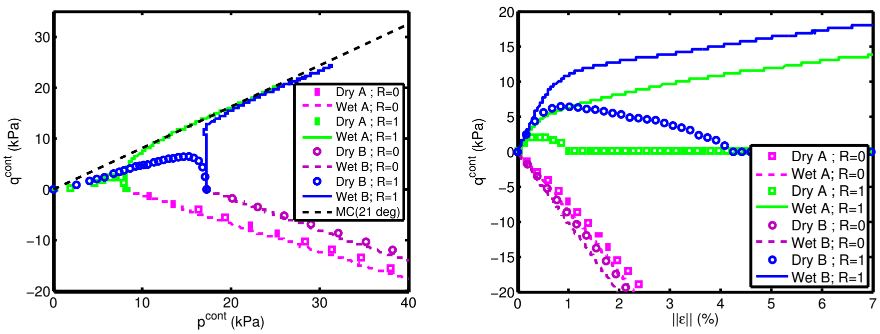

Figure 5: Contact stress response of a loose packing (Table 3) along contractant ($R = 0$) and isochoric ($R = 1$) strain loading paths (color version online)

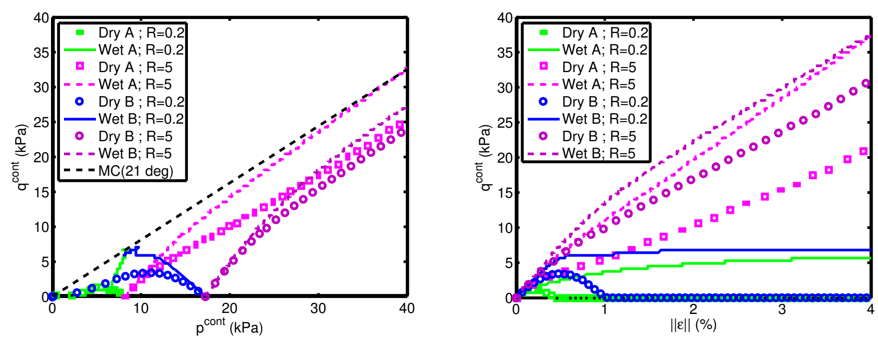

Figure 6: Contact stress response of a loose packing (Table 3) along contractant ($R = 5$) and dilatant ($R = 0.2$) strain loading paths (color version online)

similar packings under triphasic conditions gain a propensity to dilate due to liquid bridges, thus leading the mean contact stress to increase.

Some influence of the mean contact stress on the dry-wet comparison is finally observed along the dilatant loading path $R = 0.2$. Along such a path, dry conditions induce the stresses in this loose material to vanish as expected, while triphasic conditions enhance again the material dilatant nature, leading to non zero stress states. The exact behaviour of the wet material nevertheless depends on the confining pressure.

For a low confining pressure, the wet loose packing behaves similarly to the dense one because capillary stress plays an important part of the total stresses: $|p^{cap}|/p \approx 3.0$ and $|p^{cap}|/p^{cont} \approx 0.75$ at the initial stage of this test. The behaviour then changes into one with a greater propensity to dilate as a result of triphasic conditions.

On the other hand, upon increasing the confining pressure, the contact stress also increases while the capillary stress remains fairly constant, leading to $|p^{cap}|/p^{cont} \approx 0.42$ and $|p^{cap}|/p \approx 0.72$, initially. The changes in the relative contributions from contact and capillary stresses diminish the liquid bridge induced dilatancy in the loose packing.

Finally, and as previously noted for the dense packing, the plastic limit criterion ($c = 0$ Pa ; $\varphi = 21^{\circ}$) corresponding to this loose material under dry conditions [15] also applies to the contact stress under triphasic conditions, once again confirming the stress-strength effective nature of $\boldsymbol{\sigma^{cont}}$.

4.3. Discussion: effective stress vs dissipation and elasticity

The influences of the loading path and the solid packing on the ability of $\boldsymbol{\sigma^{cont}}$ to act as a stress-strain effective stress are now interpreted in relation to the variable dissipation associated with the observed behaviours. From f_n^c and f_t^c the normal and tangential components of the contact forces $\vec{f^c}$, the specific elastic energy e^{el} of the material is:

$$e^{el} = \frac{1}{2\,V} \sum_{N_c} \left(\frac{(f_n^c)^2}{k_n} + \frac{(f_t^c)^2}{k_t} \right) \tag{21}$$

which is easily measured from the DEM model, together with its increment δe^{el} between successive states. Comparing this increment with the incremental external work $\boldsymbol{\Sigma} : \boldsymbol{d\varepsilon}$, the following quantity λ quantifies the deviation of the mechanical behaviour of any dry test from a non-dissipative behaviour:

$$\lambda = \left| \frac{\boldsymbol{\Sigma} : \boldsymbol{d\varepsilon} - \delta e^{el}}{\boldsymbol{\Sigma} : \boldsymbol{d\varepsilon}} \right| \tag{22}$$

The quasi-static nature of the loading paths ensures that both the kinetic energy and the energy term associated to numerical damping are negligible, and thus do not contribute to the energy balance quantified by the quantity λ. As such, during a non-dissipative, e.g. elastic, dry loading path, λ is equal to 0 throughout since all external work is completely stored as elastic energy. On the other hand, increasing values of λ reveal an increasing dissipation. It is noted that λ may be greater than 1 in the instance of elastic energy loss ($\delta e^{el} < 0$).

However, it is to stress out that a non-dissipative behaviour with negligible values of λ does not necessarily correspond to a stress-strain path being reversible, even though the opposite is true. These intricacies are specific to granular materials whose elastic energy is contained in a contact network whose properties (for instance, N_c in Eq. (21)) fundamentally depend on irreversible strains. Also, granular materials are prone to irreversible yet non-dissipative local mechanisms such as contact losses. These very specific features can be interpreted in terms of a locked elastic energy concept [29] and have also been widely commented, e.g. in [30, 31], motivating here the distinction between the "non-dissipative" and "elastic" terminologies.

From the evolutions of λ shown in Figs. 7, and comparing with previous Figs. 3, it clearly appears that it is along the less dissipative loading paths that the stress-strain effective nature of $\boldsymbol{\sigma^{cont}}$ is the most marked, e.g. $R = 0$. Such a result includes and extends the finding previously reported in [4, 13] that an effective stress approach is possible in the elastic regime.

Another illustration of the role of dissipation in the effective stress discussion is proposed in Fig. 8 which considers an extreme case of the DEM model, referred to as $\mu = \infty$. In this extreme case of the DEM model, an ideal contact

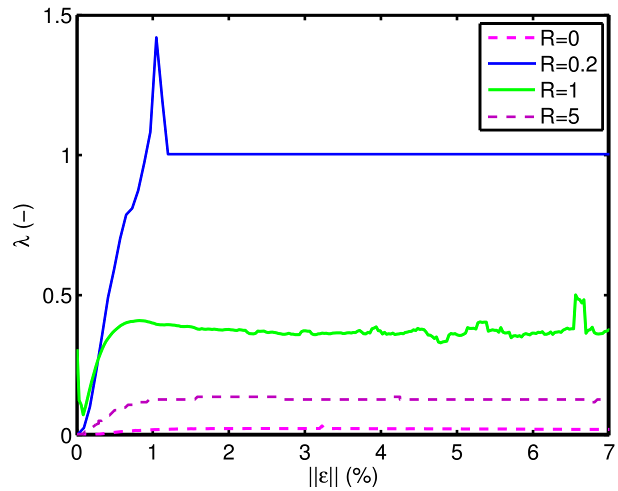

Figure 7: Dissipative nature of the behaviour during various dry loading paths imposed on the dense packing (Tests A). Raw data have been smoothed without altering the average trends and λ-values for R=0.2 may be disregarded beyond $||\boldsymbol{\varepsilon}|| \approx 1\%$ since stresses vanish at this point

description is adopted in which no frictional threshold (10) limit is imposed on the shear contact force: f_t^c just evolves linearly with the tangential relative displacement according to the shear stiffness k_t as long as a contact exists. The dry-wet comparisons shown in Fig. 8 then reveal an enhanced stress-strain effective character of $\boldsymbol{\sigma}^{\boldsymbol{cont}}$ with this model, as opposed to the already discussed dry-wet comparisons with the classical friction coefficient $\mu = 0.5$ for the loose packing along the $R = 5$ loading path.

The present discussion finally sheds some light on the generality of thermomechanical approaches to effective stress, as proposed e.g. in [23, 32, 33]. Because the effective stress discussion herein appears to be widely different depending on the elastic or dissipative nature of the behaviour, and since such thermomechanical approaches usually rely on the assumption of an elastic behaviour for the solid phase with an appropriate potential, it is probably impossible to generalize the conclusions obtained through thermomechanics outside the assumed framework.

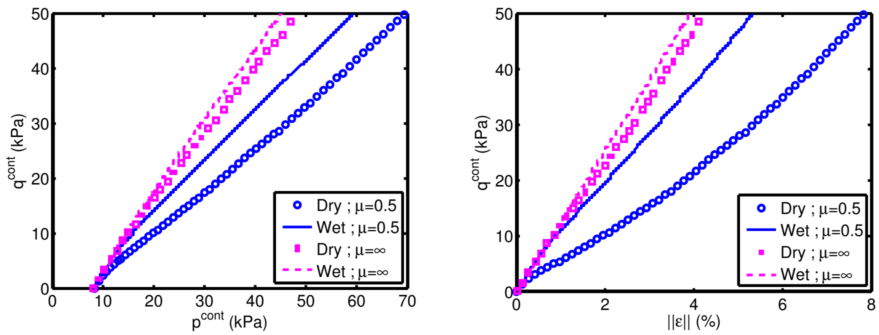

Figure 8: Influence of local friction μ on the contact stress' effective nature for a loose packing along a contractant loading path ($R = 5$)

5. Comparison with Bishop's stress

5.1. Qualitative discussion

The present μUNSAT approach to effective stress is now compared with the commonly used effective stress expression as Bishop's stress $\boldsymbol{\sigma^{Bish}}$:

$$\boldsymbol{\sigma}' \stackrel{?}{=} \boldsymbol{\sigma^{Bish}} = \boldsymbol{\Sigma} - u_n\,\boldsymbol{\delta} + u_c\,\chi\,\boldsymbol{\delta} \tag{23}$$

Formally, significant differences appear between Bishop's equation (23) and the proposed μUNSAT equation (5). It is herein recalled that the μUNSAT equation includes a surface tension dependency in addition to that of capillary pressure, as well as the possibility of a non-spherical, microstructure-dependent, capillary stress contribution. Such features that characterize the microstructural details in triphasic materials go beyond the scope of Bishop's stress that relies on an average fluid pressure, being proportionnal to u_c and necessarily spherical. Since triphasic conditions by nature involve fluid-fluid interfaces and corresponding surface tension, the lack of γ^{nw} in Bishop's approach is questionable, as is the hypothesis of an averaged (isotropic) fluid pressure, while the wetted solid surfaces for instance experience capillary pressure along their normals only. Actually, the deviatoric nature of the capillary stresses has been repeatedly demonstrated in the pendular regime from modelling approaches [6, 26, 8, 24, 20], with possible variations in q^{cont} or q^{cap} independently of q

during microstructural changes of the fluid phases, contrary to Bishop's general equality between q and q^{Bish}.

5.2. Quantitative discussion

In order to illustrate the inadequacy of Bishop's stress to serve as an effective stress in the pendular regime, other dry-wet comparisons are presented for the dense packing along the two loading paths $R \in \{1; 5\}$, from initial states presented in Table 4. The present discussion actually narrows down to the classical choice $\chi = S_w$ for Bishop's parameter, which can be continuously measured during DEM simulations thanks to the complete description of the microstructure. As such, the stress response observed in dry conditions is now compared to the Bishop's stress response measured during triphasic conditions along the same strain paths.

	Dry	Wet
Initial p (kPa)	11.5	10
Imposed u_c (kPa)	—	125
Initial S_w (%)	—	0.85
Initial n (-)	0.375	0.373
Initial z_c (-)	6.41	6.52

Table 4: Tests data for the dry-wet comparison in terms of Bishop's stress

Such loading paths $R \in \{1; 5\}$ revealed a very good agreement of the $\boldsymbol{\sigma^{cont}}$–$\boldsymbol{\varepsilon}$ behaviours in both dry and wet conditions (Figs. 3 and 4). However, the wet behaviour in terms of Bishop's stress here significantly deviates from the dry behaviour (Fig. 9), clearly showing that Bishop's stress is a much less appropriate effective stress measure along these loading paths than the contact stress. In addition to this degraded stress-strain effective character of Bishop's stress, it is also clear from the present comparison that Bishop's stress is also inadequate to describe the strength of wet materials from the dry plastic limit criterion, which $\boldsymbol{\sigma^{Bish}}$ violates. The consideration of Bishop's stress in an effective stress approach with some dry shear strength criterion in practice would thus lead to an overestimation of the risk of material failure in the pendular regime, in

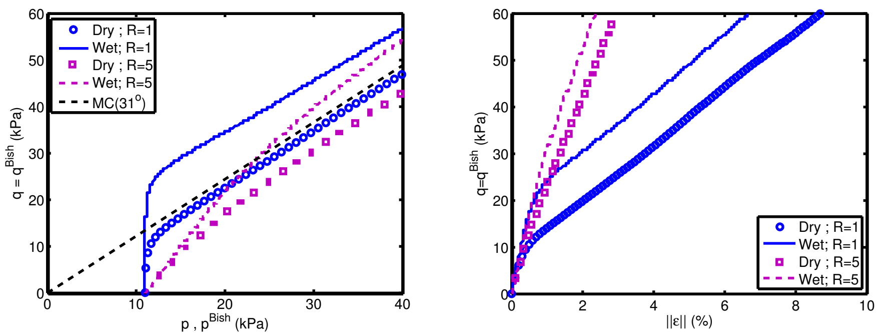

Figure 9: Bishop's or total stress responses along isochoric ($R = 1$) and contractant ($R = 5$) loading paths imposed on a dense packing

connection with an underestimation of capillary stresses already discussed in [20, 24].

6. Conclusion

Micromechanical modelling approaches showed evidence of a single effective stress variable that can be used together with dry constitutive relations to describe the strains of idealized slightly polydisperse granular media in the pendular regime. The appropriate variable is the contact stress whose direct evaluation requires the prior knowledge of the contact force network. Using the proposed μUNSAT expression, contact stresses can be alternatively calculated through measurements or estimations of the fluid phase microstructure (interconnects), which are easier to determine than forces.

Unique contact stress-strain relationships have indeed been numerically demonstrated along a variety of loading paths for both dry and wet (pendular regime) conditions. This lends strong support to applying the effective stress designation to contact stress. However, the considered loading paths have to induce small dissipation for the stress-strain effective stress approach to hold. Namely, contractant loading paths and dense packings are well suited for the application of the present μUNSAT approach to hold.

Previous experimental and phenomenological works by [4, 13] had restricted the existence of a single stress-strain effective stress in triphasic media to the elastic regime. This work based on microstructural analysis suggests a less restrictive condition by extending it to even the irreversible regime but with small dissipation.

There remain open questions as to whether new definitions of strain quantities could cast the presented results into an even more general framework. The present approach actually relies on observable strains or particle relative displacements that are due to both contact and capillary forces, through the classical DEM workflow (second Newton's law). Alternatively, it could be attempted to define distinct, non-observable, strain components: first, a contact strain uniquely caused by contact forces, and second, a capillary strain uniquely due to capillary forces, with the combination of the two leading to the observable strains herein considered. Such an alternative framework may lead to strictly unique constitutive relations between the contact stress and such a contact strain, and shed some light on the dissipation role through the yet to be defined link between contact strain and observable strain.

Acknowledgements

This work has been funded by the Natural Science and Engineering Research Council of Canada and Foundation Computer Modelling Group.

[1] K. Terzaghi, The shearing resistance of saturated soils and the angle between the planes of shear, in: Proceedings of the 1st International conference on soil mechanics and foundation engineering, Vol. 1, Cambridge, 1936, pp. 54–56.

[2] M. A. Biot, General theory of three-dimensional consolidation, Journal of Applied Physics 12 (2) (1941) 155–164. doi:10.1063/1.1712886.

[3] A. W. Bishop, G. E. Blight, Some aspects of effective stress in saturated and partly saturated soils, Géotechnique 13 (1963) 177–197.

[4] N. Khalili, F. Geiser, G. Blight, Effective stress in unsaturated soils: Review

with new evidence, International Journal of Geomechanics 4 (2) (2004) 115–126. doi:10.1061/(ASCE)1532-3641(2004)4:2(115).

[5] N. Lu, W. Likos, Suction stress characteristic curve for unsaturated soil, Journal of Geotechnical and Geoenvironmental Engineering 132 (2) (2006) 131–142. doi:10.1061/(ASCE)1090-0241(2006)132:2(131).

[6] P.-Y. Hicher, C. Chang, A microstructural elastoplastic model for unsaturated granular materials, International Journal of Solids and Structures 44 (7-8) (2007) 2304 – 2323. doi:10.1016/j.ijsolstr.2006.07.007.

[7] M. Nuth, L. Laloui, Effective stress concept in unsaturated soils: Clarification and validation of a unified framework, International Journal for Numerical and Analytical Methods in Geomechanics 32 (7) (2008) 771–801. doi:10.1002/nag.645.

[8] R. Wan, J. Duriez, F. Darve, A tensorial description of stresses in triphasic granular materials with interfaces, Geomechanics for Energy and the Environment 4 (2015) 73–87. doi:10.1016/j.gete.2015.11.004.

[9] I. Cavarretta, I. Rocchi, M. Coop, A new interparticle friction apparatus for granular materials, Canadian Geotechnical Journal 48 (12) (2011) 1829–1840. doi:10.1139/t11-077.

[10] K. Senetakis, M. R. Coop, M. C. Todisco, The inter-particle coefficient of friction at the contacts of leighton buzzard sand quartz minerals, Soils and Foundations 53 (5) (2013) 746–755. doi:10.1016/j.sandf.2013.08.012.

[11] D. G. Fredlund, N. R. Morgenstern, R. A. Widger, The shear strength of unsaturated soils, Canadian Geotechnical Journal 15 (3) (1978) 313–321. doi:10.1139/t78-029.

[12] E. E. Alonso, A. Gens, A. Josa, A constitutive model for partially saturated soils, Géotechnique 40 (3) (1990) 405–430.

[13] E. Alonso, J.-M. Pereira, J. Vaunat, S. Olivella, A microstructurally based effective stress for unsaturated soils, Géotechnique 60 (2010) 913–925(12). doi:10.1680/geot.8.P.002.

[14] W. Baille, S. Tripathy, T. Schanz, Effective stress in clays of various mineralogy, Vadose Zone Journal 13 (5). doi:10.2136/vzj2013.06.0112.

[15] J. Duriez, R. Wan, M. Pouragha, Partially saturated granular materials: Insights from micro-mechanical modelling, in: Proceedings of the 6th Biot Conference on Poromechanics, 2017, pp. 441–448. doi:10.1061/9780784480779.054.

[16] R. Hurley, E. Marteau, G. Ravichandran, J. E. Andrade, Extracting inter-particle forces in opaque granular materials: Beyond photoelasticity, Journal of the Mechanics and Physics of Solids 63 (2014) 154 – 166. doi:10.1016/j.jmps.2013.09.013.

[17] K. A. Culligan, D. Wildenschild, B. S. B. Christensen, W. G. Gray, M. L. Rivers, A. F. B. Tompson, Interfacial area measurements for unsaturated flow through a porous medium, Water Resources Research 40 (12). doi:10.1029/2004WR003278.

[18] J.-F. Bruchon, J.-M. Pereira, M. Vandamme, N. Lenoir, P. Delage, X-ray microtomography characterisation of the changes in statistical homogeneity of an unsaturated sand during imbibition, Géotechnique Letters 3 (2) (2013) 84–88. doi:10.1680/geolett.13.00013.

[19] J. Duriez, R. Wan, Contact angle mechanical influence for wet granular soils, Acta Geotechnica 12 (1) (2017) 67–83. doi:10.1007/s11440-016-0500-6.

[20] J. Duriez, M. Eghbalian, R. Wan, F. Darve, The micromechanical nature of stresses in triphasic granular media with interfaces, Journal of the Mechanics and Physics of Solids 99 (2017) 495–511. doi:10.1016/j.jmps.2016.10.011.

[21] M. E. Gurtin, A. I. Murdoch, A continuum theory of elastic material surfaces, Archive for Rational Mechanics and Analysis 57 (4) (1975) 291–323. doi:10.1007/BF00261375.

[22] X. Chateau, L. Dormieux, Homogenization of a non-saturated porous medium: Hill's lemma and applications, C. R. Acad. Sci. Paris, Série II 320 (1995) 627–634.

[23] W. G. Gray, B. A. Schrefler, Analysis of the solid phase stress tensor in multiphase porous media, International Journal for Numerical and Analytical Methods in Geomechanics 31 (4) (2007) 541–581. doi:10.1002/nag.541.

[24] J. Duriez, R. Wan, Stress in wet granular media with interfaces via homogenization and discrete element approaches, Journal of Engineering Mechanics 142 (12). doi:10.1061/(ASCE)EM.1943-7889.0001163.

[25] V. Šmilauer, et al., Yade Documentation 2nd ed, The Yade Project, 2015. doi:10.5281/zenodo.34073.
URL http://yade-dem.org/doc/

[26] L. Scholtès, P.-Y. Hicher, F. Nicot, B. Chareyre, F. Darve, On the capillary stress tensor in wet granular materials, International Journal for Numerical and Analytical Methods in Geomechanics 33 (10) (2009) 1289–1313. doi:10.1002/nag.767.

[27] S. Herminghaus, Dynamics of wet granular matter, Advances in Physics 54 (3) (2005) 221–261. doi:10.1080/00018730500167855.

[28] J. Duriez, R. Wan, Subtleties in discrete-element modelling of wet granular soils, Géotechnique 67 (4) (2017) 365–370. doi:10.1680/jgeot.15.P.113.

[29] I. F. Collins, The concept of stored plastic work or frozen elastic energy in soil mechanics, Géotechnique 55 (5) (2005) 373–382. doi:10.1680/geot.2005.55.5.373.

[30] R. Puebla, A. Relaño, Irreversible processes without energy dissipation in an isolated Lipkin-Meshkov-Glick model, Phys. Rev. E 92 (2015) 012101. doi:10.1103/PhysRevE.92.012101.

[31] M. Pouragha, R. Wan, Non-dissipative structural evolutions in granular materials within the small strain range, International Journal of Solids and Structures 110111 (2017) 94 – 105. doi:10.1016/j.ijsolstr.2017.01.039.

[32] A. Madeo, F. dell'Isola, F. Darve, A continuum model for deformable, second gradient porous media partially saturated with compressible fluids, Journal of the Mechanics and Physics of Solids 61 (11) (2013) 2196 – 2211. doi:10.1016/j.jmps.2013.06.009.

[33] E. Nikooee, G. Habibagahi, S. Hassanizadeh, A. Ghahramani, Effective stress in unsaturated soils: A thermodynamic approach based on the interfacial energy and hydromechanical coupling, Transport in Porous Media 96 (2) (2013) 369–396. doi:10.1007/s11242-012-0093-y.